

First-principles study on the electronic structure of $\text{Pb}_{10-x}\text{Cu}_x(\text{PO}_4)_6\text{O}$ ($x=0, 1$)

Junwen Lai,^{1,2,*} Jiangxu Li,^{1,*} Peitao Liu,^{1,†} Yan Sun,^{1,‡} and Xing-Qiu Chen¹

¹Shenyang National Laboratory for Materials Science, Institute of Metal Research,
Chinese Academy of Sciences, 110016 Shenyang, China.

²School of Materials Science and Engineering, University of Science and Technology of China, 110016 Shenyang, China.

Recently, Lee *et al.* reported the experimental discovery of room-temperature ambient-pressure superconductivity in a Cu-doped lead-apatite (LK-99) (arXiv:2307.12008, arXiv:2307.12037). Remarkably, the superconductivity persists up to 400 K at ambient pressure. Despite strong experimental evidence, the electronic structure of LK-99 has not yet been studied. Here, we investigate the electronic structures of LK-99 and its parent compound using first-principles calculations, aiming to elucidate the doping effects of Cu. Our results reveal that the parent compound $\text{Pb}_{10}(\text{PO}_4)_6\text{O}$ is an insulator, while Cu doping induces an insulator-metal transition and thus volume contraction. The band structures of LK-99 around the Fermi level are featured by a half-filled flat band and a fully-occupied flat band. These two flat bands arise from both the $2p$ orbitals of 1/4-occupied O atoms and the hybridization of the $3d$ orbitals of Cu with the $2p$ orbitals of its nearest-neighbor O atoms. Interestingly, we observe four van Hove singularities on these two flat bands, indicating electronic instability towards structural distortions at low temperatures. Furthermore, we show that the band energies of the van Hove singularities can be tuned by including electronic correlation effects or doping with different elements. We find that among the considered doping elements (Ni, Cu, Zn, Ag, and Au), both Ni and Zn doping result in the gap opening, whereas Au exhibits doping effects more similar to Cu than Ag. Our work provides a foundation for future studies on the role of unique electronic structures of LK-99 in superconductivity.

I. INTRODUCTION

Superconductors are highly valued in various fields due to their unique characteristics of zero resistance and perfect diamagnetism [1]. This has led experimental and theoretical scientists to tirelessly search for high- T_c superconductors, resulting in numerous breakthroughs in the field, such as the non-hydrogen BCS superconductor MgB_2 ($T_c=39$ K, ambient pressure) [2], the Cu-based unconventional superconductor Hg-Ba-Ca-O system ($T_c=133$ K, ambient pressure) [3], the Fe-based unconventional superconductor single-layer FeSe film ($T_c=77$ K, ambient pressure) [4], and the Ni-based unconventional superconductor $\text{La}_3\text{Ni}_2\text{O}_7$ ($T_c=80$ K, 14.0~43.5 GPa) [5]. Owing to Neil Ashcroft's seminal insights that metallic hydrogen under sufficiently high pressures and hydrides at lower pressures by chemical precompression may exhibit room-temperature superconductivity [6, 7], the search has turned to the superhydrides [8–24], leading to the so-called “hydride rush” [25–27]. Despite extensive research, the T_c remains below the room temperature, or the required pressure is too high, which greatly hinders practical applications. While the near-ambient superconductivity has been recently claimed in a nitrogen-doped lutetium hydride [28], its validity remains a subject of ongoing debate [29–32].

Rather than focusing on hydride superconductors, a groundbreaking discovery was recently reported by Lee *et al.* [33, 34], claiming the realization of the first room-temperature ambient-pressure superconductor in a Cu-doped lead-apatite (LK-99). The reported T_c is as high as 400 K at ambient pressure, and convincing experimental characterizations, such as resistivity, Meissner effect, and I-V character-

istics, were performed [34]. Moreover, the authors provided an exhaustive sample synthesis method, which would enable other experimental groups to readily reproduce their findings. Despite the strong experimental evidence, several important questions remain open: What are the electronic structures of the LK-99 and its parent compound, what is the role played by Cu, and is it possible to achieve similar effects through doping other elements?

In this work, we set out to address these issues using first-principle density functional theory calculations. We find that the parent compound $\text{Pb}_{10}(\text{PO}_4)_6\text{O}$ of LK-99 is an insulator exhibiting two flat bands below the Fermi level. Doping Cu induces an insulator-metal transition, which is featured by a half-filled flat band and a fully-occupied flat band around the Fermi level. These two flat bands come from both the $2p$ orbitals of 1/4-occupied O2 atoms and the hybridization of the $3d$ orbitals of Cu with the $2p$ orbitals of its nearest-neighbor O1 atoms, necessitating a minimal two-band low-energy effective model for describing LK-99. In addition, we observe four van Hove singularities (VHSs) on these two flat bands stemming from the saddle dispersions at the M and L points in the Brillouin zone. We show that the band energies of the VHSs can be tuned by electronic correlations or doping different elements. Among the considered doping elements (Ni, Cu, Zn, Ag, and Au), both Ni and Zn doping open the band gap, whereas Au exhibits doping effects more similar to Cu than Ag.

II. COMPUTATIONAL DETAILS

The first-principles calculations were performed using the Vienna *ab initio* simulation package (VASP) [35, 36]. The plane-wave cutoff was chosen to be 520 eV. A Γ -centered k -point grid with a k -spacing of $0.03\ 2\pi/\text{\AA}$ was used for structural relaxations and the k -spacing was reduced to $0.02\ 2\pi/\text{\AA}$

* These authors contribute equally to this work.

† ptliu@imr.ac.cn

‡ sunyan@imr.ac.cn

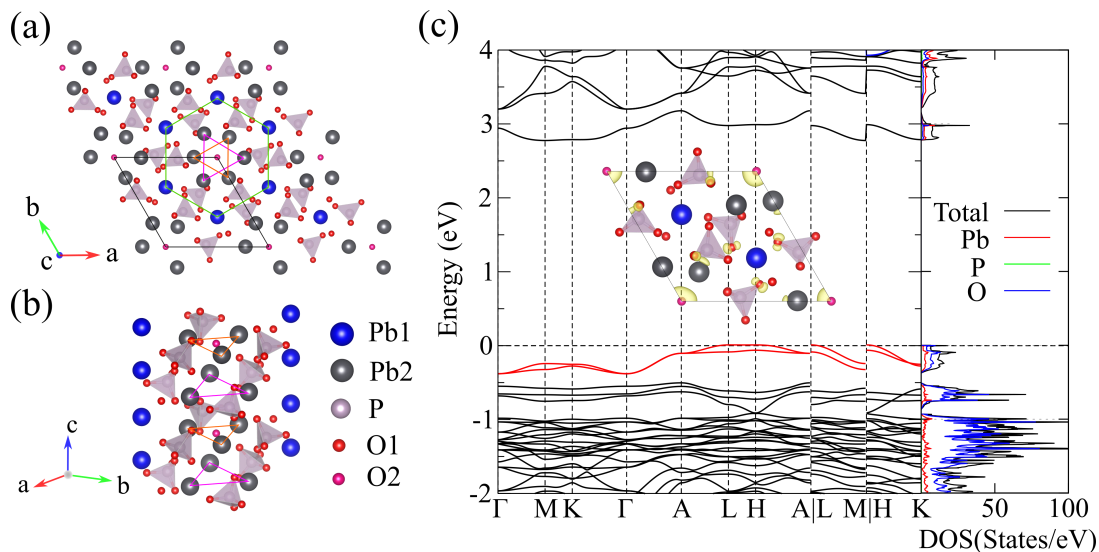


Figure 1. (a) Top view of the crystal structure of lead-apatite with a chemical formula of $\text{Pb}_{10}(\text{PO}_4)_6\text{O}$. The black lines indicate the unit cell that is periodically replicated. The Pb1 atoms form a hexagon marked by green lines. The Pb2 atoms form two oppositely shaped triangles marked by pink and orange lines. The O2 atoms are 1/4 occupied. The O1 atoms denote other O atoms (excluding O2) including the ones forming PO_4 units. (b) Side view of the crystal structure, highlighting a cylindrical column centered at O2 atoms. (c) The calculated electronic band structure and density of states. The inset shows the isosurfaces of calculated charge densities (isovalue= $0.007 \text{ e}/\text{\AA}^3$) for the two flat bands (in red color) below the Fermi level.

for density of states (DOSs) calculations, The electronic interactions were described using the Perdew-Burke-Ernzerhof (PBE) functional [37]. The VASP recommended projector augmented wave pseudopotentials [38, 39] were employed. The tetrahedron method with Blöchl corrections was used for DOSs calculations, whereas the Gaussian smearing method with a smearing width of 0.05 eV was used for other calculations. The convergence criteria for the total energy and ionic forces were set to 10^{-6} eV and $0.01 \text{ eV}/\text{\AA}$, respectively.

III. RESULTS AND DISCUSSIONS

A. Structural and electronic properties of lead-apatite

Figure 1(a) shows the crystal structure of lead-apatite with a chemical formula of $\text{Pb}_{10}(\text{PO}_4)_6\text{O}$. It is the parent compound of LK-99 with a hexagonal ($P6_3/m$, space group 176) lattice. The calculated lattice parameters are $a=10.024 \text{ \AA}$ and $c=7.482 \text{ \AA}$, in good agreement with the experimental values ($a=9.865 \text{ \AA}$ and $c=7.431 \text{ \AA}$) [40]. The predicted larger lattice parameters arise from the overestimation of the employed PBE functional. In the lead-apatite, there exists two symmetry-inequivalent Pb atoms, named Pb1 and Pb2. The Pb1 atoms form a hexagon, whereas the Pb2 atoms form two oppositely shaped triangles [see Fig. 1(a)]. Along the c axis, the Pb2 atoms along with the surrounding PO_4 units form a cylindrical column centered at O2 atoms [see Fig. 1(b)]. We note that the O2 atoms are 1/4 occupied. To simulate this, we removed three out of four O2 atoms in calculations. The employed structure is provided in the Supplementary Mater-

ial [41].

The calculated electronic band structure and DOSs of lead-apatite are shown in Fig. 1(c). It is obvious that the lead-apatite is an insulator with a PBE-predicted indirect gap of 2.77 eV. The obtained insulating nature of lead-apatite is consistent with the experimental observations [33, 34]. It should be stressed that the 1/4 occupation of O2 atoms is important to open the band gap. Full occupation of O2 atoms results in a metallic state. DOSs show that the valence bands below the Fermi level are contributed by the dominate O-2p states and minor Pb-6p states. Two flat bands right below the Fermi level are observed. The calculated charge densities reveal that they are mainly from the O2 atoms and first-nearest-neighboring O1 atoms of Pb1 atoms [insert of Fig. 1(c)].

B. Electronic structure of LK-99

Having analyzed structural and electronic properties of lead-apatite, we turn to LK-99. In experiment, the LK-99 exhibits a chemical formula of $\text{Pb}_{10-x}\text{Cu}_x(\text{PO}_4)_6\text{O}$ with $0.9 < x < 1.1$ [34]. Furthermore, it was found that the Cu atoms occupy the Pb1 positions in the crystal structure [34]. For simplicity, we only considered the case with $x=1$, which can be achieved by substituting a Pb1 atom with a Cu atom, resulting in $\text{Pb}_9\text{Cu}(\text{PO}_4)_6\text{O}$. We note that Cu doping induces symmetry breaking, resulting in four possible configurations (see Supplementary Material Fig. S1 [41]). These configurations have total energies that are very close to each other ($< 5 \text{ meV}/\text{atom}$), but in this study, we focus on the configuration with the lowest energy, whose crystal structure is shown in Figs. 2(a) and (b)

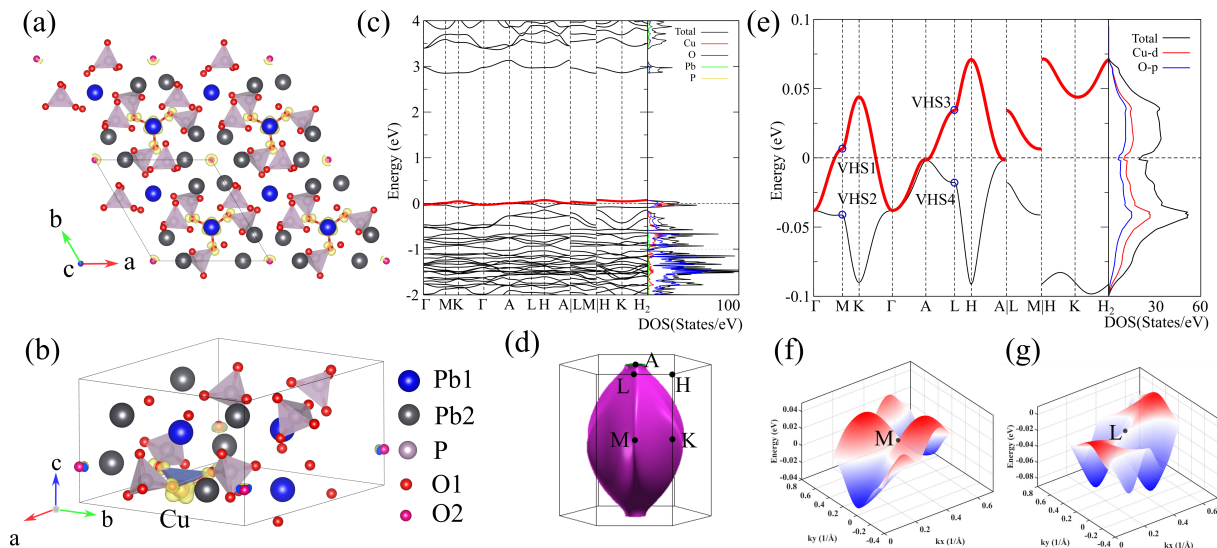


Figure 2. (a, b) Top and side views of the crystal structure of LK-99 with a chemical formula of $\text{Pb}_9\text{Cu}(\text{PO}_4)_6\text{O}$. Here, the isosurfaces of calculated charge densities (isovalue= $0.011 \text{ e}/\text{\AA}^3$) for the two flat bands around the Fermi level [red lines in (c)] are superimposed. (c) The calculated electronic band structure and density of states. (d) The computed Fermi surface. (e) Zoom-in of (c), highlighting the half-filled flat band and four VHSs marked by VHS1 and VHS2 at M and VHS3 and VHS4 at L. (f, g) The three-dimensional visualizations of the half-filled flat band around the M and L points, respectively, highlighting the saddle dispersions around VHS1 and VHS3. Note that all the results here were obtained using PBE without taking into account on-site Coulomb interactions on the d shell of Cu.

Table I. The PBE predicted lattice parameters a and c (in \AA), volume (in \AA^3), and band gap (in eV) of $\text{Pb}_9\text{M}(\text{PO}_4)_6\text{O}$ where M indicates the elements listed below. Note that M=Pb corresponds to the parent compound of LK-99.

M	a	c	Volume	Band gap
Pb	10.024	7.482	651.02	2.77
Expt.[40]	9.865	7.431	626.25	Insulator
Cu	9.931	7.411	632.94	Metal
Expt.[34]	9.843	7.428	623.24	Metal
Ni	9.815	7.386	616.29	2.92
Zn	9.833	7.384	618.34	0.82
Ag	9.941	7.382	631.69	Metal
Au	9.928	7.421	633.48	Metal

and provided in the Supplementary Material [41]. The calculated lattice parameters of LK-99 ($a=9.931 \text{ \AA}$ and $c=7.411 \text{ \AA}$) are in good agreement with the experimental values ($a=9.843 \text{ \AA}$ and $c=7.428 \text{ \AA}$) [34]. As compared to the non-doped lead-apatite, Cu doping results in a 2.9% reduction of the system volume (Table I) due to the insulator-metal transition, which was argued as one of the key factors contributing to the realization of room-temperature superconductivity in LK-99 [34].

Figures 2(c) and (e) show the calculated band structure and DOSs of LK-99. Clearly, after Cu doping, the LK-99 becomes metallic, with just one half-filled very flat band (dispersion $< 0.1 \text{ eV}$) crossing the Fermi level. The Fermi surface looks like a rugby and consists of both electron and hole pockets [Fig. 2(d)]. Below this half-filled flat band there exists another flat band that is fully occupied. In contrast to

the widely studied one-band Hubbard model applicable to cuprates [42, 43], here a minimal two-band low-energy effective model should be used to describe the physics of LK-99, since the two flat bands are contributed by both the $2p$ states of O2 atoms and the hybridization of the Cu- $3d$ states with the $2p$ states of its first-nearest-neighboring O1 atoms [see Figs. 2(a) and (b)]. It is interesting to note that the conduction electrons are confined in the layer containing doped Cu atoms, whereas other layers without doped Cu atoms seem insulating. In addition, the PO_4 units surrounding the cylindrical column formed by Pb2 atoms also exhibit insulating characteristics, leading to a one-dimensional-like conduction channel along the c axis mediated by the 1/4-occupied O2 atoms. More interestingly, we observed four VHSs on these two flat bands, originating from the saddle dispersions at the M and L points in the Brillouin zone [see Figs. 2(e), (f) and (g)]. This indicates that the electronic properties are fragile in response to structural distortions at low temperatures. The existence of these peculiar flat bands may be connected with the experimentally observed remarkable superconducting properties of LK-99 [33, 34], which warrants further investigation.

Before closing this section, we briefly discuss the effects of electronic correlations on the band structures. As mentioned earlier, Cu doping leads to the formation of a half-filled flat band and a fully-occupied flat band around the Fermi level, which are suggestive of strong electronic correlations. Figure 3 compares the two flat bands and DOSs around the Fermi level with and without on-site Coulomb interactions on the d shell of Cu. We used an effective Hubbard U of 4 eV [44] based on the Dudarev scheme [45]. The results show that inclusion of the Hubbard interactions slightly shifts the two flat

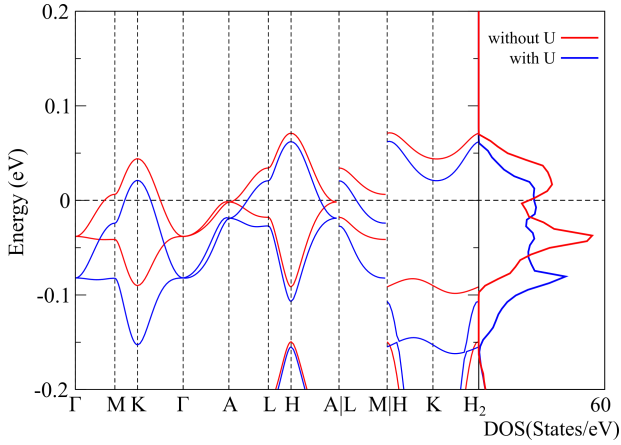


Figure 3. Effects of electronic correlations on the band structures and total density of states of LK-99 around the Fermi level.

bands to lower energies and increases the bandwidth, which is somewhat unusual as Hubbard interactions typically localize electrons and decrease the bandwidth. These findings suggest that electronic correlations can fine-tune the band structures around the Fermi level and have an impact on the superconducting properties.

C. Electronic structure tuning via different elements doping

As previously introduced, LK-99 exhibits novel electronic structures around the Fermi level that may play a crucial role in forming its superconducting state. A natural question arises as to whether these novel electronic structures are a result of the specific Cu doping, or in other words, whether alternative elements exist having similar doping effects to Cu. To address this question, we conducted first-principles band structure calculations using different doping elements. Specifically, we considered four elements: Ni, Zn, Ag, and Au. Ni and Zn are located on the left and right sides of Cu, respectively, in the periodic table, and we chose them to examine the effects of electron filling. Ag and Au belong to the same group as Cu, and we included them to investigate the effects of volume.

Figures 4(a) and (b) show that both Ni and Zn doping result in gap opening. This can be understood from the electron filling, since both elements lead to the even number of valence electrons. Turning to the Ag and Au doping cases, one can see from Figs. 4(c) and (d) that the two flat bands around the Fermi level persist due to their similar electronic configurations as Cu (note the small energy scale). However, we find that the doping effects of Au are more similar to Cu than those of Ag. This observation may be explained by the closer volumes between Au-doped and Cu-doped lead-apatites (see Table I). It is worth mentioning that, compared to Cu, Au doping further narrows the two flat bands, brings the VHS1 at the M point and VHS3 at the L point closer to the Fermi level, and results in larger DOSs around the Fermi level [see Figs. 4(c) and (d)]. These results suggest that Au-doped lead-

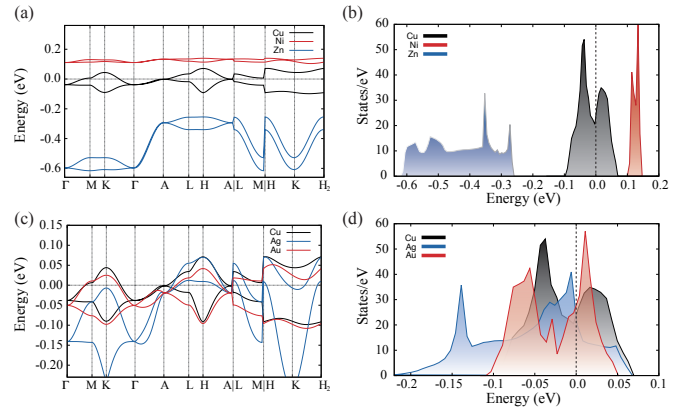


Figure 4. Effects of different elements doping on the (a, c) band structures and (b, d) total density of states of LK-99 around the Fermi level. Note that all the results here were obtained using PBE without taking into account on-site Coulomb interactions on the d shell.

apatite may also exhibit similar superconducting properties as the Cu-doped one.

IV. CONCLUSIONS

In conclusion, we have performed a thorough first-principles electronic structure analysis of both LK-99 and its parent compound. Our results demonstrate that the parent compound without doping is an insulator with a large band gap. Cu doping closes the band gap, resulting in an insulator-metal transition and volume contraction. The band structures of LK-99 exhibit novel characteristics around the Fermi level, which are manifested by the presence of a half-filled flat band and a fully-occupied flat band with two VHSs each. These two flat bands arise from both the $2p$ orbitals of $1/4$ -occupied O2 atoms and the hybridization of the $3d$ orbitals of Cu with the $2p$ orbitals of its nearest-neighbor O1 atoms, necessitating a minimal two-band low-energy effective model. The former $2p$ orbitals of $1/4$ -occupied O2 atoms lead to a one-dimensional-like cylindrical conduction channel along the c axis surrounded by insulating PO_4 units, whereas the latter hybridized Cu- $3d$ orbitals and O1- $2p$ orbitals give rise to a two-dimensional-like electron charge distribution in the ab -plane. The observed VHSs are robust against electronic correlation effects and their band energies can be tuned by doping different elements. We find that Au exhibits doping effects more similar to Cu than Ag. We anticipate that the distinctive electronic structures of LK-99 that we observed in this study will aid in identifying the source of its exceptional superconducting properties.

V. ACKNOWLEDGMENTS

This work was supported by the National Key R&D Program of China (No. 2021YFB3501503), the National Nat-

- [1] P. Mangin and R. Kahn, *Superconductivity: An introduction* (Springer Cham, New York, 2016).
- [2] J. Nagamatsu, N. Nakagawa, T. Muranaka, Y. Zenitani, and J. Akimitsu, *Nature* **410**, 63 (2001).
- [3] A. Schilling, M. Cantoni, J. D. Guo, and H. R. Ott, *Nature* **363**, 56 (1993).
- [4] W. Qing-Yan, L. Zhi, Z. Wen-Hao, Z. Zuo-Cheng, Z. Jin-Song, L. Wei, D. Hao, O. Yun-Bo, D. Peng, C. Kai, W. Jing, S. Can-Li, H. Ke, J. Jin-Feng, J. Shuai-Hua, W. Ya-Yu, W. Li-Li, C. Xi, M. Xu-Cun, and X. Qi-Kun, *Chinese Physics Letters* **29**, 037402 (2012).
- [5] H. Sun, M. Huo, X. Hu, J. Li, Z. Liu, Y. Han, L. Tang, Z. Mao, P. Yang, B. Wang, J. Cheng, D.-X. Yao, G.-M. Zhang, and M. Wang, *Nature* (2023), 10.1038/s41586-023-06408-7.
- [6] N. W. Ashcroft, *Phys. Rev. Lett.* **21**, 1748 (1968).
- [7] N. W. Ashcroft, *Phys. Rev. Lett.* **92**, 187002 (2004).
- [8] Y. Li, J. Hao, H. Liu, Y. Li, and Y. Ma, *The Journal of Chemical Physics* **140**, 174712 (2014).
- [9] D. Duan, Y. Liu, F. Tian, D. Li, X. Huang, Z. Zhao, H. Yu, B. Liu, W. Tian, and T. Cui, *Scientific Reports* **4**, 6968 (2014).
- [10] A. P. Drozdov, M. I. Erements, I. A. Troyan, V. Ksenofontov, and S. I. Shylin, *Nature* **525**, 73 (2015).
- [11] A. P. Drozdov, P. P. Kong, V. S. Minkov, S. P. Besedin, M. A. Kuzovnikov, S. Mozaffari, L. Balicas, F. F. Balakirev, D. E. Graf, V. B. Prakapenka, E. Greenberg, D. A. Knyazev, M. Tkacz, and M. I. Erements, *Nature* **569**, 528 (2019).
- [12] M. Somayazulu, M. Ahart, A. K. Mishra, Z. M. Geballe, M. Baldini, Y. Meng, V. V. Struzhkin, and R. J. Hemley, *Phys. Rev. Lett.* **122**, 027001 (2019).
- [13] D. V. Semenov, A. G. Kvashnin, A. G. Ivanova, V. Svitlyk, V. Y. Fomin, A. V. Sadakov, O. A. Sobolevskiy, V. M. Pudalov, I. A. Troyan, and A. R. Oganov, *Materials Today* **33**, 36 (2020).
- [14] I. A. Troyan, D. V. Semenov, A. G. Kvashnin, A. V. Sadakov, O. A. Sobolevskiy, V. M. Pudalov, A. G. Ivanova, V. B. Prakapenka, E. Greenberg, A. G. Gavriluk, I. S. Lyubutin, V. V. Struzhkin, A. Bergara, I. Errea, R. Bianco, M. Calandra, F. Mauri, L. Monacelli, R. Akashi, and A. R. Oganov, *Advanced Materials* **33**, 2006832 (2021).
- [15] E. Snider, N. Dasenbrock-Gammon, R. McBride, X. Wang, N. Meyers, K. V. Lawler, E. Zurek, A. Salamat, and R. P. Dias, *Phys. Rev. Lett.* **126**, 117003 (2021).
- [16] Z. Zhang, T. Cui, M. J. Hutcheon, A. M. Shipley, H. Song, M. Du, V. Z. Kresin, D. Duan, C. J. Pickard, and Y. Yao, *Phys. Rev. Lett.* **128**, 047001 (2022).
- [17] Y. Song, J. Bi, Y. Nakamoto, K. Shimizu, H. Liu, B. Zou, G. Liu, H. Wang, and Y. Ma, *Phys. Rev. Lett.* **130**, 266001 (2023).
- [18] D. V. Semenov, I. A. Kruglov, I. A. Savkin, A. G. Kvashnin, and A. R. Oganov, *Current Opinion in Solid State and Materials Science* **24**, 100808 (2020).
- [19] X. Zhang, Y. Zhao, F. Li, and G. Yang, *Matter and Radiation at Extremes* **6**, 068201 (2021).
- [20] Y. Sun, J. Lv, Y. Xie, H. Liu, and Y. Ma, *Phys. Rev. Lett.* **123**, 097001 (2019).
- [21] S. Di Cataldo, W. von der Linden, and L. Boeri, *Phys. Rev. B* **102**, 014516 (2020).
- [22] N. Geng, T. Bi, and E. Zurek, *The Journal of Physical Chemistry C* **126**, 7208 (2022).
- [23] A. D. Grockowiak, M. Ahart, T. Helm, W. A. Coniglio, R. Kumar, K. Glazyrin, G. Garbarino, Y. Meng, M. Oliff, V. Williams, N. W. Ashcroft, R. J. Hemley, M. Somayazulu, and S. W. Tozer, *Frontiers in Electronic Materials* **2**, 837651 (2022).
- [24] S. Di Cataldo and L. Boeri, *Phys. Rev. B* **107**, L060501 (2023).
- [25] J. Lv, Y. Sun, H. Liu, and Y. Ma, *Matter and Radiation at Extremes* **5**, 068101 (2020).
- [26] J. A. Flores-Livas, L. Boeri, A. Sanna, G. Profeta, R. Arita, and M. Erements, *Physics Reports* **856**, 1 (2020).
- [27] B. Lilia, R. Hennig, P. Hirschfeld, G. Profeta, A. Sanna, E. Zurek, W. E. Pickett, M. Amsler, R. Dias, M. I. Erements, C. Heil, R. J. Hemley, H. Liu, Y. Ma, C. Pierleoni, A. N. Kolmogorov, N. Rybin, D. Novoselov, V. Anisimov, A. R. Oganov, C. J. Pickard, T. Bi, R. Arita, I. Errea, C. Pellegrini, R. Requist, E. K. U. Gross, E. R. Margine, S. R. Xie, Y. Quan, A. Hire, L. Fanfarillo, G. R. Stewart, J. J. Hamlin, V. Stanev, R. S. Gonnelli, E. Piatti, D. Romanin, D. Daghero, and R. Valenti, *Journal of Physics: Condensed Matter* **34**, 183002 (2022).
- [28] N. Dasenbrock-Gammon, E. Snider, R. McBride, H. Pasan, D. Durkee, N. Khalvashi-Sutter, S. Munasinghe, S. E. Dissanayake, K. V. Lawler, A. Salamat, and R. P. Dias, *Nature* **615**, 244 (2023).
- [29] X. Ming, Y.-J. Zhang, X. Zhu, Q. Li, C. He, Y. Liu, T. Huang, G. Liu, B. Zheng, H. Yang, J. Sun, X. Xi, and H.-H. Wen, *Nature* (2023), 10.1038/s41586-023-06162-w.
- [30] X. Xing, C. Wang, L. Yu, J. Xu, C. Zhang, M. Zhang, S. Huang, X. Zhang, B. Yang, X. Chen, Y. Zhang, J. gang Guo, Z. Shi, Y. Ma, C. Chen, and X. Liu, *arXiv:2303.17587* (2023).
- [31] N. P. Salke, A. C. Mark, M. Ahart, and R. J. Hemley, *arXiv:2306.06301* (2023).
- [32] D. Peng, Q. Zeng, F. Lan, Z. Xing, Y. Ding, and H. kwang Mao, *arXiv:2307.00201* (2023).
- [33] S. Lee, J.-H. Kim, and Y.-W. Kwon, *arXiv:2307.12008* (2023).
- [34] S. Lee, J. Kim, H.-T. Kim, S. Im, S. An, and K. H. Auh, *arXiv:2307.12037* (2023).
- [35] G. Kresse and J. Hafner, *Phys. Rev. B* **47**, 558 (1993).
- [36] G. Kresse and J. Furthmüller, *Phys. Rev. B* **54**, 11169 (1996).
- [37] J. P. Perdew, K. Burke, and M. Ernzerhof, *Phys. Rev. Lett.* **77**, 3865 (1996).
- [38] P. E. Blöchl, *Phys. Rev. B* **50**, 17953 (1994).
- [39] G. Kresse and D. Joubert, *Phys. Rev. B* **59**, 1758 (1999).
- [40] S. V. Krivovichev and P. C. Burns, *Zeitschrift für Kristallographie - Crystalline Materials* **218**, 357 (2003).
- [41] See Supplemental Material for the detailed information on employed structure models.
- [42] E. Gull and A. J. Millis, *Nature Physics* **11**, 808 (2015).
- [43] H.-C. Jiang and T. P. Devereaux, *Science* **365**, 1424 (2019).
- [44] L. Wang, T. Maxisch, and G. Ceder, *Phys. Rev. B* **73**, 195107 (2006).
- [45] S. L. Dudarev, G. A. Botton, S. Y. Savrasov, C. J. Humphreys, and A. P. Sutton, *Phys. Rev. B* **57**, 1505 (1998).

Supplementary Material to
“First-principles study on the electronic structure of $\text{Pb}_{10-x}\text{Cu}_x(\text{PO}_4)_6\text{O}$ ($x=0, 1$)”

Junwen Lai,^{1,2,*} Jiangxu Li,^{1,*} Peitao Liu,^{1,†} Yan Sun,^{1,‡} and Xing-Qiu Chen¹

¹*Shenyang National Laboratory for Materials Science, Institute of Metal Research,
Chinese Academy of Sciences, 110016 Shenyang, China.*

²*School of Materials Science and Engineering, University of Science and Technology of China, 110016 Shenyang, China.*

arXiv:2307.16040v1 [cond-mat.mtrl-sci] 29 Jul 2023

* These authors contribute equally to this work.

† ptliu@imr.ac.cn

‡ sunyan@imr.ac.cn

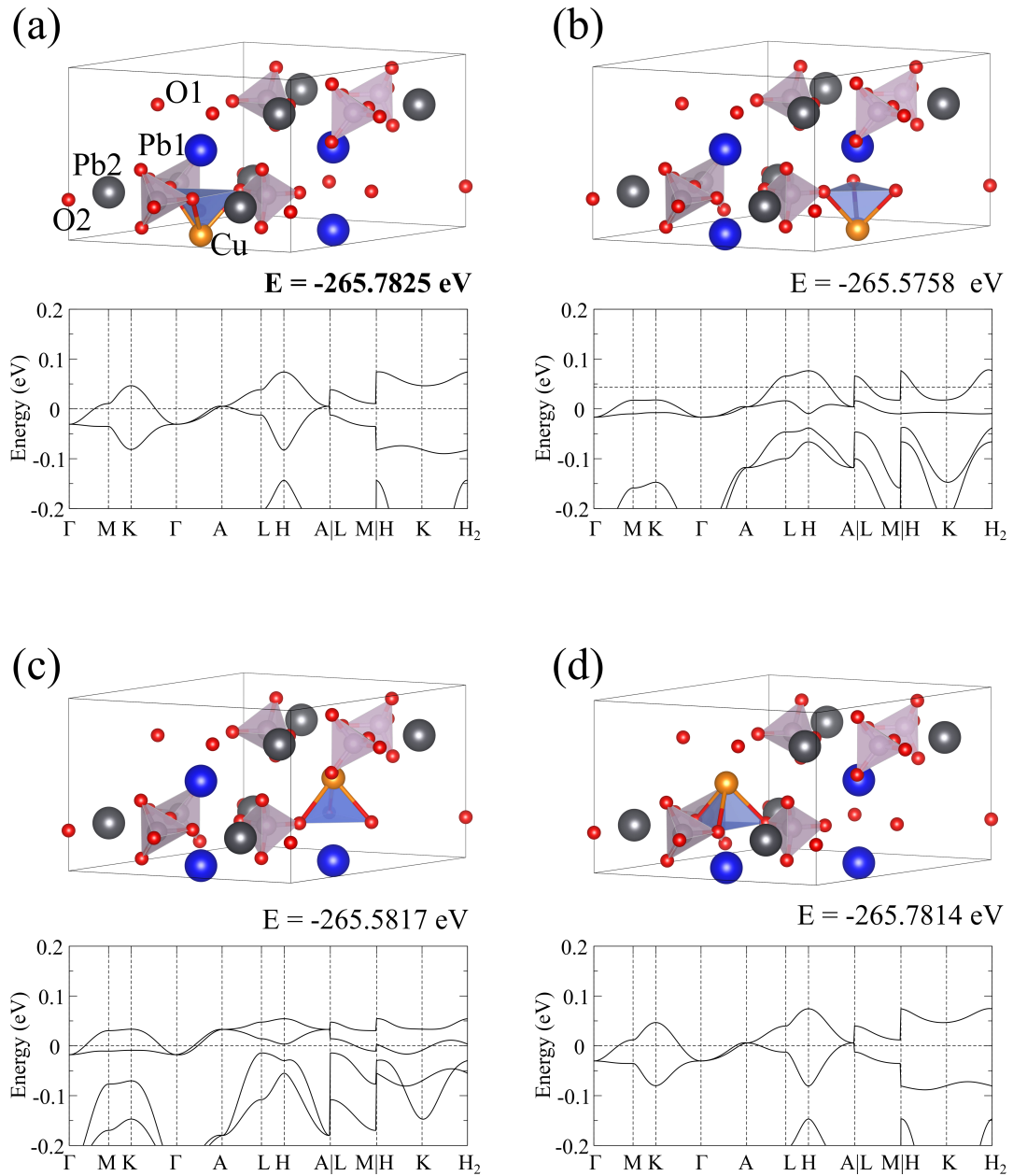


Figure S1. Crystal and band structures of four possible lead-apatite configurations with a Cu atom substituting a Pb1 site. From the band structures, it seems that (a) and (d) are symmetry-equivalent configurations, and (b) and (c) are symmetry-equivalent configurations. In any case, there exist two flat bands crossing the Fermi level. The energies difference between (a) and (b) are small (< 5 meV/atom). The adopted Cu-doped structure model [i.e., Fig. 2(b) of the main text] corresponds to the configuration (a) here.

Pb10(P04)60

1.0000000000000000		
10.0239401044820102	0.0000006121514461	0.0000000000000000
-5.0119705824320677	8.6809864704190467	0.0000000000000000
0.0000000000000000	0.0000000000000000	7.4815041019845081

Pb P O

10 6 25

Direct

0.9963538867363795	0.7711561244778835	0.2443294850732514
0.0050062123768200	0.2643090859692521	0.7464431433615388

0.2288438755221165	0.2251977622584960	0.2443294850732514
0.7356909140307479	0.7406971274075715	0.7464431433615388
0.7748022527415088	0.0036461272636217	0.2443294850732514
0.2593028875924333	0.9949938016231812	0.7464431433615388
0.6666666870000029	0.3333334299999996	0.0042634124695411
0.3333333129999971	0.6666662699999979	0.0072229018756005
0.3333333129999971	0.6666662699999979	0.4870401649864249
0.6666666870000029	0.3333334299999996	0.4951010130162885
0.6239014908271940	0.5947299148479956	0.2487979403241596
0.3668872594614285	0.3950708418260263	0.7483756092457483
0.4052700851520044	0.0291715459791888	0.2487979403241596
0.6049291581739737	0.9718164476354048	0.7483756092457483
0.9708284840208137	0.3760985391728084	0.2487979403241596
0.0281835823645977	0.6331127705385740	0.7483756092457483
0.5006906503976367	0.6458112695516860	0.2472504771707875
0.4689633991493309	0.3196890005137618	0.7495392298128181
0.3541887304483140	0.8548793808459507	0.2472504771707875
0.6803109994862382	0.1492743976355726	0.7495392298128181
0.1451205891540468	0.4993093206023573	0.2472504771707875
0.8507255723644249	0.5310365718506631	0.7495392298128181
0.7292899627055505	0.6547134078302221	0.0796661284193476
0.2609217265457389	0.3521073372121108	0.9164206285216281
0.3452865921697779	0.0745765248753330	0.0796661284193476
0.6478926627878892	0.9088144183336340	0.9164206285216281
0.9254235041246730	0.2707100672944520	0.0796661284193476
0.0911856106663720	0.7390783034542636	0.9164206285216281
0.2583831295645709	0.3475865624117134	0.5824263589771803
0.7304908854720296	0.6591553131478420	0.4164438897440874
0.6524134375882866	0.9107965961528564	0.5824263589771803
0.3408446868521580	0.0713355423241993	0.4164438897440874
0.0892034328471496	0.7416169004354316	0.5824263589771803
0.9286644866758067	0.2695091445279658	0.4164438897440874
0.5445286861139778	0.4147734915236683	0.2515084873369702
0.4721921906908833	0.5767053663538633	0.7451733587211393
0.5852264784763292	0.1297551945903166	0.2515084873369702
0.4232946036461342	0.8954867643370079	0.7451733587211393
0.8702447754096809	0.4554713138860222	0.2515084873369702
0.1045132056629896	0.5278078093091167	0.7451733587211393
0.0000000000000000	0.0000000000000000	0.2339466544173519

Pb9Cu(P04)60

1.0000000000000000

9.9306823821051555 -0.0000014818366361 0.0000000000000000

-4.9653399077953200 8.6002239607356703 -0.0000000000000000

0.0000000000000000 0.0000000000000000 7.4109945172796605

Pb	Cu	P	O
9	1	6	25

Direct

0.9986807449642078 0.7699202447216552 0.2474756380877509

0.9977014382162520 0.2577003216124319 0.7545056960306785

0.2300797552783452 0.2287605002425670 0.2474756380877509

0.7422996783875685 0.7400011176038168 0.7545056960306785

0.7712395147574378 0.0013192690357936 0.2474756380877509

0.2599988973961879 0.0022985757837491 0.7545056960306785

0.3333333129999971 0.6666662699999979 0.0102252768912011

0.3333333129999971 0.6666662699999979 0.4962563424132084

0.6666666870000029 0.3333334299999996 0.5217140548665616

0.6666666870000029 0.3333334299999996 0.0634955699714910

0.6238378061607577 0.5940989414527301 0.2330614375419467

0.3715115645822017	0.3913852574380640	0.7499251076346213
0.4059010585472700	0.0297388347080183	0.2330614375419467
0.6086147425619355	0.9801263371441329	0.7499251076346213
0.9702611952919840	0.3761622238392447	0.2330614375419467
0.0198736928558696	0.6284884654178010	0.7499251076346213
0.4970341950086190	0.6419127807282180	0.2504819573050943
0.4722574174374839	0.3124116086150668	0.7489819492636393
0.3580872192717823	0.8551214142804011	0.2504819573050943
0.6875883913849331	0.1598458078224275	0.7489819492636393
0.1448785557195963	0.5029657759913753	0.2504819573050943
0.8401541621775773	0.5277425535625101	0.7489819492636393
0.7465890784344098	0.6974373665162791	0.0877326196589775
0.2518710331486960	0.3302579489920529	0.9082269759127742
0.3025626334837207	0.0491516819181211	0.0877326196589775
0.6697420510079468	0.9216131131566275	0.9082269759127742
0.9508483470818850	0.2534109515655927	0.0877326196589775
0.0783869158433784	0.7481289968513065	0.9082269759127742
0.2751067320564097	0.3631086026138700	0.5737407252403873
0.7132743878686607	0.6201447197159712	0.4140528338576862
0.6368913973861298	0.9119981584425314	0.5737407252403873
0.3798552802840290	0.0931296381526946	0.4140528338576862
0.0880018705574747	0.7248932979435926	0.5737407252403873
0.9068703908473114	0.2867256421313418	0.4140528338576862
0.5441603686812513	0.4191736441937305	0.1764358135764958
0.4780900223868556	0.5733419996779769	0.7722935441387523
0.5808263258062671	0.1249867244875282	0.1764358135764958
0.4266579703220141	0.9047479627088743	0.7722935441387523
0.8750132455124694	0.4558396313187486	0.1764358135764958
0.0952520072911234	0.5219099776131445	0.7722935441387523
-0.0000000000000000	0.0000000000000000	0.2917658511111268

Pb9Ni(P04)60

1.0000000000000000

9.8154531593033294	0.0000006796980621	0.0000000000000001
-4.9077271683365957	8.5004314457636099	-0.0000000000000000
-0.0000000000000000	0.0000000000000000	7.3864048600067536

Pb Ni P O
9 1 6 25

Direct

0.0023930570875375	0.7740062083079475	0.2599301159193992
0.9981263570376689	0.2484453590588505	0.7611097394955972
0.2259937916920525	0.2283868487795829	0.2599301159193992
0.7515546409411493	0.7496809989788294	0.7611097394955972
0.7716131662204218	0.9976069569124635	0.2599301159193992
0.2503190160211756	0.0018736569623321	0.7611097394955972
0.3333333129999971	0.6666666269999979	0.0083563744589139
0.3333333129999971	0.6666666269999979	0.4916993729060725
0.6666666870000029	0.3333333429999996	0.4939887254346352
0.6666666870000029	0.3333333429999996	0.9888074251107263
0.6266506161499268	0.5918699199409470	0.2244060791164619
0.3812271863310681	0.3914807614839344	0.7587825215394234
0.4081300800590461	0.0347806662089776	0.2244060791164619
0.6085192385160657	0.9897464548471361	0.7587825215394234
0.9652193637910250	0.3733494138500756	0.2244060791164619
0.0102535751528665	0.6187728436689346	0.7587825215394234
0.4897391594662527	0.6281642336558425	0.2489403253336887
0.4820546686219311	0.3088652905428651	0.7673862121357911
0.3718357663441578	0.8615749258104103	0.2489403253336887

0.6911347094571351	0.1731893770790694	0.7673862121357911
0.1384250441895871	0.5102608115337415	0.2489403253336887
0.8268105929209353	0.5179453023780702	0.7673862121357911
0.7518336521017459	0.7139248061257816	0.0902259672136851
0.2562082985300035	0.3329554348200832	0.9124466916157625
0.2860751938742185	0.0379088159759619	0.0902259672136851
0.6670445651799166	0.9232528927099121	0.9124466916157625
0.9620912130240441	0.2481663778982495	0.0902259672136851
0.0767471362900938	0.7437917314699990	0.9124466916157625
0.2895518375743092	0.3595968242700853	0.5775506773213896
0.7126740787308330	0.6140434059575414	0.4093799310935214
0.6404031757299147	0.9299550423042227	0.5775506773213896
0.3859565940424590	0.0986306427732962	0.4093799310935214
0.0700449866957832	0.7104481924257007	0.5775506773213896
0.9013693862267099	0.2873259512691698	0.4093799310935214
0.5607077621046025	0.4217205963411343	0.1527077813282273
0.4884167698367849	0.5753387950552064	0.7771070179708647
0.5782793736588628	0.1389871657634679	0.1527077813282273
0.4246611749447841	0.9130779147815733	0.7771070179708647
0.8610128042365367	0.4392922378953977	0.1527077813282273
0.0869220552184240	0.5115832301632152	0.7771070179708647
0.0000000000000000	-0.0000000000000000	0.3314289118382008

Pb9Zn(P04)60

1.0000000000000000

9.8334400401958248

0.0000006480018838

0.0000000000000000

-4.9167205813333723

8.5160085573994344

-0.0000000000000000

0.0000000000000000

-0.0000000000000000

7.3839056703763655

Pb	Zn	P	O
9	1	6	25

Direct

0.0019823826540479	0.7745389833574755	0.2605685968567902
0.0005492517510040	0.2495094521966610	0.7609281354007629
0.2254610166425249	0.2274433992965728	0.2605685968567902
0.7504905478033389	0.7510398005543468	0.7609281354007629
0.7725566157034323	0.9980176313459532	0.2605685968567902
0.2489602144456582	0.9994507622489972	0.7609281354007629
0.3333333129999971	0.6666666269999979	0.0092920421241173
0.3333333129999971	0.6666666269999979	0.4917023846699586
0.6666666870000029	0.3333333429999996	0.4879616587832145
0.6666666870000029	0.3333333429999996	0.9847445792127363
0.6259143338516501	0.5933171010070440	0.2252532299041020
0.3822381133433937	0.3922924244537182	0.7580217383289192
0.4066828989929561	0.0325972028445967	0.2252532299041020
0.6077075755462819	0.9899457188896851	0.7580217383289192
0.9674028271554057	0.3740856961483525	0.2252532299041020
0.0100543111103175	0.6177619166566158	0.7580217383289192
0.4910937622588408	0.6322733513223806	0.2499554912148296
0.4847413266035737	0.3119647511826648	0.7673767206525192
0.3677266486776189	0.8588204109364665	0.2499554912148296
0.6880352488173350	0.1727765744209266	0.7673767206525192
0.1411795590635306	0.5089062087411530	0.2499554912148296
0.8272233955790783	0.5152586443964203	0.7673767206525192
0.7513852734009998	0.7147244060386004	0.0905765954240719
0.2568117601649497	0.3325059740779390	0.9112845865311741
0.2852755939613921	0.0366608373623969	0.0905765954240719
0.6674940259220613	0.9243058150869953	0.9112845865311741
0.9633391916376089	0.2486147565989954	0.0905765954240719

0.0756942139130106	0.7431882698350526	0.9112845865311741
0.2907901127615214	0.3596347159378105	0.5766867280958088
0.7120123182191316	0.6147601473879272	0.4101790717415690
0.6403652840621893	0.9311554258237027	0.5766867280958088
0.3852398526120730	0.0972521408312160	0.4101790717415690
0.0688446031763033	0.7092099172384810	0.5766867280958088
0.9027478881687901	0.2879877117808713	0.4101790717415690
0.5600593234989890	0.4238839768242669	0.1541878947238398
0.4880216222353552	0.5759472461580564	0.7770246166653357
0.5761159931757306	0.1361753466747224	0.1541878947238398
0.4240527238419343	0.9120743160772867	0.7770246166653357
0.8638246233252747	0.4399406765010177	0.1541878947238398
0.0879256539227108	0.5119783777646448	0.7770246166653357
0.0000000000000000	-0.0000000000000000	0.3343691085908144

Pb9Ag(P04)60

1.0000000000000000

9.9406156256295830	0.0000014316309071	-0.0000000000000000
-4.9703090526946276	8.6088249452360159	0.0000000000000000
0.0000000000000000	0.0000000000000000	7.3815177070995590

Pb	Ag	P	O
9	1	6	25

Direct

0.9955447579595498	0.7644045746843522	0.2509353602597195
0.9949927298849605	0.2573394633408910	0.7433247032096960
0.2355954253156481	0.2311401832752049	0.2509353602597195
0.7426605366591089	0.7376532675440730	0.7433247032096960
0.7688598317247997	0.0044552560404515	0.2509353602597195
0.2623467474559317	0.0050072841150407	0.7433247032096960
0.6666666870000029	0.3333333429999996	0.0097937783126133
0.3333333129999971	0.6666666269999979	0.9965361097111132
0.3333333129999971	0.6666666269999979	0.4835217433780268
0.6666666870000029	0.3333333429999996	0.5070448998213292
0.6224543720111532	0.5948504549204371	0.2525617534221464
0.3707022294599365	0.3908319789848494	0.7434265012518808
0.4051495450795629	0.0276038870907134	0.2525617534221464
0.6091680210151508	0.9798702804750824	0.7434265012518808
0.9723961429092889	0.3775456579888496	0.2525617534221464
0.0201297495249200	0.6292978005400662	0.7434265012518808
0.5033527712042026	0.6535305546234698	0.2412930483724593
0.4710849401433576	0.3119139273367794	0.7495567696311050
0.3464694453765302	0.8498222165807333	0.2412930483724593
0.6880860726632205	0.1591710118065815	0.7495567696311050
0.1501777534192646	0.4966471997957914	0.2412930483724593
0.8408289581934234	0.5289150308566359	0.7495567696311050
0.7183250028016291	0.6312858593131695	0.0733313605171702
0.2695585902134868	0.3589354917114473	0.9170778206359134
0.3687141406868311	0.0870391134884577	0.0733313605171702
0.6410645082885525	0.9106231275020309	0.9170778206359134
0.9129609155115483	0.2816750271983734	0.0733313605171702
0.0893769014979748	0.7304414397865158	0.9170778206359134
0.2548561473055233	0.3330481904549279	0.5805447120393449
0.7420730616480391	0.6836840845297045	0.4069712237348472
0.6669518095450727	0.9218079858505874	0.5805447120393449
0.3163159154702953	0.0583889471183460	0.4069712237348472
0.0781920431494186	0.7451438826944794	0.5805447120393449
0.9416110818816598	0.2579269683519635	0.4069712237348472
0.5370078419806492	0.4163530057402559	0.2864992188809570

0.4776500244900591	0.5727569085520745	0.7251055610784928
0.5836469642597415	0.1206548362403932	0.2864992188809570
0.4272430614479162	0.9048930559379801	0.7251055610784928
0.8793451337596041	0.4629921580193508	0.2864992188809570
0.0951069140620176	0.5223499755099412	0.7251055610784928
0.0000000000000000	0.0000000000000000	0.2254193596757327

Pb9Au(P04)60

1.0000000000000000

9.9283792820894288 0.0000013290778343 -0.0000000000000001

-4.9641907921107915 8.5982280121573389 -0.0000000000000000

0.0000000000000000 -0.0000000000000000 7.4206648327525606

Pb Au P O

9 1 6 25

Direct

0.9987233766629506 0.7700297440372798 0.2448161471961586

0.9969578478045801 0.2566428143246935 0.7388207969009422

0.2299702559627202 0.2286936326256779 0.2448161471961586

0.7433571856753066 0.7403150344798909 0.7388207969009422

0.7713063823743271 0.0012766373370507 0.2448161471961586

0.2596849805201143 0.0030421661954207 0.7388207969009422

0.6666666870000029 0.3333333429999996 0.0135593361795980

0.3333333129999971 0.6666666269999979 0.9968935070071225

0.3333333129999971 0.6666666269999979 0.4811144980220491

0.6666666870000029 0.3333333429999996 0.5126567045891999

0.6240235712206006 0.5957989341703960 0.2567762672942094

0.3725888757357917 0.3916743705957365 0.7421386506787645

0.4042010658296044 0.0282246070502167 0.2567762672942094

0.6083256294042633 0.9809145351400576 0.7421386506787645

0.9717754229497860 0.3759764587794018 0.2567762672942094

0.0190854948599448 0.6274111542642108 0.7421386506787645

0.4984971284963468 0.6460404521305081 0.2409835588602634

0.4733875116231799 0.3117224796945201 0.7500784349250454

0.3539595478694922 0.8524566763658462 0.2409835588602634

0.6882775203054801 0.1616650309286632 0.7500784349250454

0.1475432936341515 0.5015028425036472 0.2409835588602634

0.8383349390713415 0.5266124593768144 0.7500784349250454

0.7157264128121672 0.6264516885192809 0.0762573986474450

0.2765938771727317 0.3645903707883150 0.9178508294109737

0.3735483114807189 0.0892746942928838 0.0762573986474450

0.6354096292116850 0.9120035353844084 0.9178508294109737

0.9107253347071221 0.2842736171878352 0.0762573986474450

0.0879964936155975 0.7234061528272706 0.9178508294109737

0.2537416035714394 0.3286511177541609 0.5839074550456410

0.7447503840873385 0.6950959851918572 0.4051645076649013

0.6713488822458390 0.9250905148172633 0.5839074550456410

0.3049040148081429 0.0496543688954859 0.4051645076649013

0.0749095141827429 0.7462584264285628 0.5839074550456410

0.9503456601045199 0.2552496459126570 0.4051645076649013

0.5439737144232027 0.4184961225329676 0.3021575567533752

0.4798450214250294 0.5729385081852881 0.7170648712999956

0.5815038474670371 0.1254775918902420 0.3021575567533752

0.4270614618147026 0.9069064532397367 0.7170648712999956

0.8745223781097555 0.4560262855767976 0.3021575567533752

0.0930935167602609 0.5201549785749704 0.7170648712999956

0.0000000000000000 0.0000000000000000 0.2019265201688183